RSC Advances

ROYAL SOCIETY OF CHEMISTRY

www.rsc.org/advances

Understanding the electron density reorganization upon stacking vs H-bonding interaction in methyl gallate-caffeine complexes.

*Laura Estévez, Marta Sánchez-Lozano, Ricardo A. Mosquera**

Departamento de Química Física, Facultade de Química, Universidade de Vigo, Lagoas-Marcosende s/n 36310-Vigo (Galicia, Spain)

*Corresponding author. E-mail: mosquera@uvigo.es

Abstract

The crystal structure of methyl gallate/caffeine complex combines H-bonding and π-π stacking interactions, becoming a model case to get insight about the joint effect of these intermolecular interactions on electronic reorganization. Selected subcomplexes contained in this crystal structure were subjected to analysis by using the Quantum Theory of Atoms in Molecules, QTAIM. This analysis in complexes formed through stacking reveals that a small amount of electron density is transferred from methyl gallate to caffeine. The reverse charge transference (CT), in larger extent, takes place in in-plane H-bonding complexes. In-plane CTs dominate in complexes showing both kinds of interactions. Cooperative effects are nearly negligible when caffeine is surrounded by methyl gallate molecules, while they become significant in complexes where methyl gallate is placed in the central position. This different behavior can be explained considering the H-bonds established between caffeine units in the latter complexes. QTAIM analysis also indicates that stacking interactions are characterized

by a depletion of the electron density in the intermonomer region and a modification of their atomic quadrupole moments.

1. Introduction

Molecular organization and molecular interactions are the basis of the functional properties of most molecules. Molecular recognition processes are influenced by many different factors which make their study complicated. For example, the anti-Alzheimer´s drug Aricept utilizes π-π, O-H/π, and cation-π interactions in its binding.[1] Furthermore, these interactions are difficult to study experimentally because they often occur in complex systems where secondary interactions and solvent effects can complicate the interpretation of results.[2] Additionally, precise gas-phase studies of small model systems are often challenging[3] because of the weak binding and the flatness of the potential energy landscape, which can lead to rapid interconversion of structures which are close in energy. Progress requires a quantitative understanding of these different factors. Some relevant interactions between functional groups, such as H-bonding, are well-understood, however, the picture for weaker less well-defined interactions is not so clear, e.g. those between aromatic groups.

An improved understanding of non-covalent interactions would greatly aid to the rational design of supramolecular architectures, crystal engineering, or predicting relationships between chemical structure and function useful in drug design. In principle, theoretical quantum mechanical models are very useful in this regard because they can directly provide the intrinsic strength of these interactions. The combination of the computational levels required for obtaining an accurate description of stacking complexes and the size of these systems complicated for years the studies on this kind of non-covalent interactions. Nevertheless, the reliability of the results provided by

recent kinetic-optimized DFT functionals[4,5] has provided a useful tool for obtaining electron densities in these systems.

In this work, we have selected one crystal structure available in the Cambridge Crystal Structure Database, CCSD, reported by Martin et al.[6] It consists of methyl gallate and caffeine monomers, whose in-plane complexation is built by hydrogen bonding, where both monomers are able to act as H-donor and H-acceptor, while π-π interactions are responsible for stacked structure. Methyl gallate is recognized as a good antioxidant belonging to the polyphenols family. Caffeine is a xanthine alkaloid, commonly found in mild stimulants and bronchodilators.[7] Methyl gallate-caffeine is an example of the stacking complexes considered for explaining diverse properties of polyphenols[8] where the structure is well known,[6,9] what unfortunately is far from being a general case.

By using this system, we attempt to describe from an electronic point of view how the π-π interaction takes place and cooperative effects among the diverse interactions (π-π or hydrogen bonding) present on the crystal structure analyzed. With this purpose, we have carried out an electron density analysis with the Quantum Theory of Atoms in Molecules (QTAIM),[10,11] which is considered among the most reliable tools of modern electron density analysis. Previously, QTAIM has provided insight into the electronic origin of several chemical basic features[10-12] like: approximate transferability,[13-17] diverse conformational preferences,[18,19] hydrogen bonding,[20-23] strain energy,[14,24] characterization of intermolecular interactions,[25] etc.

Computational Details

The good performance of the MPW1B95/6-311++G(2d,2p) 6d level for describing stacking complexes was proved in quinhydrone.[26] Thus, we employ this computational

level here to study methyl gallate···caffeine complexes. The geometries for the systems studied here were extracted from the crystal structure[6] available in the CCSD, where every methyl gallate molecule, **M**, is surrounded in its plane by three molecules of caffeine, **C**. Reciprocally, every **C** molecule is surrounded coplanarly by three **M**. The in-plane intermolecular structure is mainly due to three different kinds of intermolecular hydrogen bonds (IHB): O3'-H3'···O6 (complex **1**), O5'-H5'···O1 (complex **2**) and O4'-H4'···N9 (complex **3**), (Figure 1). We have also considered the complex formed by one **C** unit surrounded in the same plane by 3 **M** units (complex **4**) and that formed by one **M** unit surrounded by 3 in-plane **C** ones (complex **5**), (Figure 1).

Furthermore, in the crystal, planes are displaced to allow face to face π-π interactions where every **C** is stacked between two **M** and vice versa. Therefore, we have also considered systems formed by one caffeine molecule and one of its closest out of plane **M** neighbors. Although, each monomer displays the same orientation and geometry in all the planes, neither the methyl groups of **M** nor those of **C** are eclipsed to the corresponding back bone plane. Thus, two different **M**···**C** stacked units are found in the crystal. They are denoted as **6** and **7** in Figure 2. Complex **6** displays eight hydrogens in the intermolecular region whereas there are only four in **7**. This difference is noteworthy, resulting in shorter plane to plane distances for the latter complex (3.49 Å *vs*. 3.61 Å). Two additional stacking complexes formed by three molecules were also studied to analyze cooperative effects. Thus, in complex **8** one **C** molecule is placed between two **M** ones (**C**···**M**···**C**), whereas **9** represents the reciprocal complex (**M**···**C**···**M**). Finally, looking for cooperative effects between in plane H-bonding and π-π interactions, we studied the complexes where **C** is surrounded by three in-plane **M** units and other two in face to face arrangements, **10**, and that where **M** is connected to five **C** ones, **11** (Figure 3).

Single-point calculations, in the geometry of the crystal, with the MPW1B95 functional[27] were carried out using the 6-311++G(2d,2p) 6d basis set with Gaussian 03 program[28] for all the complexes described above (**1**-**11**) as well as for the **C** and **M** monomers. Comparison of electron densities, $\rho(\mathbf{r})$ obtained for a certain X complex, $\rho^{X}(\mathbf{r})$, and the summation of those computed for its constituting fragments, $\rho^{i}(\mathbf{r})$, (i= **M**, **C**), is provided through electron deformation density, $\Delta\rho(\mathbf{r})$, plots (Eq. 1).

$$\Delta\rho(\mathbf{r})= \rho^{X}(\mathbf{r}) - \Sigma_i\rho^{i}(\mathbf{r}) \qquad \{1\}$$

In each molecule, the QTAIM electron density analysis was performed with the AIMPAC[29] package of programs and AIM2000.[30] In this work we focus on the properties at the bond critical points (BCP) of $\rho(\mathbf{r})$:[10,11] Electron density, $\rho(\mathbf{r_c})$, its Laplacian, $\nabla^2\rho(\mathbf{r_c})$, and the value of the total energy density, $H(\mathbf{r_c})$.[31] We also discuss some of the atomic properties provided by integrating $\rho(\mathbf{r})$ over atomic basins: atomic electron population, $N(\Omega)$, atomic energy, $E(\Omega)$, the first vectorial moment of the atomic electron density, $\mu(\Omega)$, with its module and components; the first and second scalar moments of $\rho(\mathbf{r})$ with regard to atomic nucleus, $r^1(\Omega)$ and $r^2(\Omega)$, atomic volumes computed making use of 10^{-3} au, $v_1(\Omega)$, and $2\cdot10^{-3}$ au, $v_2(\Omega)$, and the corresponding electron populations enclosed by them, $N_1(\Omega)$ and $N_2(\Omega)$, as well as that part of $N(\Omega)$ placed between both isosurfaces, $N_{12}(\Omega)$, the elements of the matrix of the atomic electron quadrupole moment, $Q_{ij}(\Omega)$, especially $Q_{zz}(\Omega)$ where z represents an axis that is always orthogonal to the ring of monomers, and finally, the atomic Shannon entropy of the electron distribution, $Sh(\Omega)$.[32,33]

The accuracy obtained in the determination of the integrated properties was checked using standard criteria. Thus, summations of $N(\Omega)$ and atomic energy, $E(\Omega)$, values for each molecule reproduce total electron populations and electronic molecular energies

within $2 \cdot 10^{-4}$ au and 1.0 kJ·mol^{-1}, respectively. No atom was integrated with absolute values of $L(\Omega)$[10,11] larger than $2 \cdot 10^{-3}$ au.

Results and Discussion

H-bonding complexes (1-5). Molecular energies for H-bonding complexes **1**-**3** and monomers, in the geometry of its corresponding complex, obtained at the MPW1B95/6-311++G(2d,2p) 6d level are given in Table 1. Binding energies (Table 1), $\Delta^b E$, indicate the most stable **M**···**C** adduct is **1**, displaying (Figure 1) an O3'-H3'···O6 intermolecular hydrogen bond (IHB). It is followed by complex **2** (7.5 kJ·mol^{-1} less stable), where O5'-H5'···O2 should be the expected IHB, and complex **3,** (16.4 kJ·mol^{-1} less stable), showing an O4'-H4'···N9 IHB. In all the complexes, the H atom involved in expected strong IHB, H^d, belongs to **M**, which could be referred as H-donor, while **C** would be the H-acceptor. Making use of QTAIM atomic energies, we observe that **C** is stabilized ($\Sigma\Delta^b E(\Omega)$= -0.5177 au in complex **1**), while **M** results destabilized ($\Sigma\Delta^b E(\Omega)$= 0.5018 au in complex **1**). The same trend is observed (data not shown) for the remaining IHB complexes (**2**-**5**).

QTAIM analysis of the electron densities obtained at the same level for each system reveals more than one intermolecular bond critical point (BCP) in each of them (Figure 1). Indeed, the analysis locates four intermolecular bond paths (IBP) in **1**, five IBPS in **2** and three in complex **3** (Figure 1: a, b and c, respectively). Thus, larger number of IHBs cannot be invoked to justify the largest stabilization of complex **1**.

Nevertheless, complex **1** displays the strongest IHB (Table 2). Besides the typical hydrogen bonds as O-H···X IHBs (X=O, N), weaker ones of the type C-H···X (X=H, O) are also characterized in Table 2. It is noticeable that **M** does not always acts as H-donor when weak IHBs are considered.

All the interactions (Table 2) are clearly of the closed-shell type exhibiting positive values of both $\nabla^2\rho(\mathbf{r}_c)$ and $H(\mathbf{r}_c)$. Values of $\rho(\mathbf{r}_c)$, $\nabla^2\rho(\mathbf{r}_c)$ and $H(\mathbf{r}_c)$ evaluated at the BCPs for typical IHBs are in the order observed for this kind of interaction. Values of BCP properties associated to weak C-H···X (X=H, O) interactions are smaller: $\rho(\mathbf{r}_c)$ values are between $3.6\cdot10^{-3}$ and $9.0\cdot10^{-3}$ au, $\nabla^2\rho(\mathbf{r}_c)$ ones are between $13.7\cdot10^{-3}$ and $35.9\cdot10^{-3}$ au. Also $H(\mathbf{r}_c)$ values are smaller, between $0.7\cdot10^{-3}$ and $1.5\cdot10^{-3}$ au. They are similar to those found in previous QTAIM works on IHB interactions in DNA bases.[34]

The variation of atomic electron populations due to IHB binding, $\Delta^b N(\Omega)$, in complexes **1**-**3** indicates that IHB complexation results in:

i) Global charge transfer (CT) from **C** monomer to **M** one (0.025, 0.020 and 0.034 au for **1**, **2**, and **3**, respectively). Thus, the electron density of H-donors increases in compounds **1**-**3** although, as usual,[21] $N(H^d)$ decreases upon IHB formation.

ii) The largest variations correspond to atoms involved in the strongest IBPs (Table 3). These variations are also observed looking at the $\Delta\rho(\mathbf{r})$ plot for HB complex **1** as is shown in Figure 4a. In the HB complex **1** (similar pictures are obtained for **2** and **3**) the deformation concentrates on the strongest intermolecular bond path, which displays alternate depletion and enhancement regions, each of them resembling a certain cylindrical symmetry, typical of IHBs.[35] Looking at this figure, we can realize that the deformation also shows the similar trend for weaker IHB. Globally, the interaction gives rise to an electron density reorganization of the whole molecule, as pointed by the results shown in Table 4.

iii) The summations of $\Delta^b N(\Omega)$ values for the atoms involved in the strongest IHB (Table 3) are negative in **M** and positive in **C**. That is, they display the reverse trend observed for global CT. Thus, as previously observed,[36] CT involved in IHB is obtained

from the rest of the H-donor (**C** in this case) and transferred to other regions of H-acceptor (**M**).

Complexes **4** and **5** allow analyzing cooperative effects among IHBs. They are slightly higher (6.8 kJ mol^{-1}) in complex **4** than in complex **5** (2.0 kJ mol^{-1}). Looking for an explanation we have compared bond paths established in complexes **1**-**3** with those of **4** and **5**. No significant changes in BCP properties are observed in **4** and **5** with regard to the corresponding BCPs in complexes **1**-**3**. Nevertheless, it has to be noticed that in complex **4**, besides the heteromonomeric IHBs between **M** monomers and central **C** one, one bifurcated C-H···O IHB is established between two **M** monomers (Figure 1). Homomonomeric intermolecular bond paths are also found in complex **5**. Nevertheless they correspond to a bifurcated H···H interaction between two **C** monomers and their $\rho(\mathbf{r}_c)$ values are one order of magnitude lower than those observed in **5** for C-H···O IHB (Figure 1). Thus, larger cooperative effects in **4** can be related to the additional C-H···O bifurcated IHB present.

There is also global CT from **C** to the three **M** monomers in **4** (0.073 au) and from the three **C** units to central **M** in **5**, where M receives 0.071 au. In **4**, each **M** receives 0.023, 0.022 and 0.029 au. In **5** each **C** unit transfers 0.025, 0.018 and 0.030 au. Thus, cooperative effects are always below ±0.005 au, being the most intense in the binding due to O4'-H4'···N9 IHB and nearly negligible in that containing the O5'-H5'···O2 IHB.

Face to face adducts (6-9). Molecular energies (Table 1) show that the stability of stacked **C**···**M** adducts, **6** and **7**, is about that shown by the least stable of the corresponding IHB adducts (complex **3**). Binding energies (-15.9 and -22.6 kJ mol^{-1}) for these adducts are larger than those obtained for face to face catechol dimer[35] and are

within the range estimated for π-stacking energies between DNA bases (10 to 30 kJ mol^{-1}).[37] Complex **6** displays ~~8~~ eight hydrogens in the intermolecular region whereas there are only ~~4~~ four in **7**.

QTAIM analysis of the MPW1B95/6-311++G(2d,2p) 6d electron density of the adduct reveals seven intermolecular BCPs (Figure 2) in both **C**···**M** complexes, although only two of them are established between the same pairs of atoms (O1''(sp^2)···N7 and O3'···H1). In accordance with previous findings in other stacking complexes,[34,37,38] all of them display positive $\nabla^2\rho(\mathbf{r_c})$ and $H(\mathbf{r_c})$ values (Table 5). In all cases $\rho(\mathbf{r_c})$, $\nabla^2\rho(\mathbf{r_c})$, and $H(\mathbf{r_c})$ values are similar to those of catechol dimer[35] and those found between DNA bases.[34] The IBP with the highest $\rho(\mathbf{r_c})$ value is the shortest one. It is found in complex **7** between O5' and one of the hydrogens of the methyl group attached to N5 in caffeine. As commented above, **M** and **C** monomers are closer in complex **7** than in **6**, whereas the latter displays a larger number of hydrogen atoms in the intermonomer region. In this case, the largest stability corresponds to the stacked complex with the shortest intermolecular distance, **7**, which is also the one displaying the largest $\rho(\mathbf{r}_c)$ value.

Integration of the electron density within each atomic basin in the stacking complex indicates a really small global CT between monomers: 0.007 au from **M** to **C**, contrasting with the electron transference from **C** to **M** in all the HB complexes here studied. Careful evaluation of atomic and bond properties for adducts **6** and **7** was done in order to assess the electronic origin of stacking interactions.

For the sake of concision we are only describing the results obtained for one of the stacked **C**···**M** adducts, as both display exactly the same qualitative trends and very similar values. Both monomers display atoms with positive and negative $\Delta^b N(\Omega)$ values, all of them of very small amount (Table 6). Although $\Delta^b N(\Omega)$ values are small and

follow a complicated trend of variation, we observe certain common trends for diverse moments of the electron density, like $\mu(\Omega)$ and $Q(\Omega)$ matrix, or statistics descriptors like $Sh(\Omega)$, (Table 6) that could be taken as an indicator of the participation of electrostatic interactions in this complex (see below).

If we focus on Δ^b variations, in general, the atoms involved in the strongest stacking IBPs (C5, N7 and H7^g in **C** and C2' and O1''(sp^2) in **M**) display large $|\Delta^b N(\Omega)|$, $|\Delta^b \mu_z(\Omega)|$, and $|\Delta^b Q_{zz}(\Omega)|$ values (Table 6 and Figure 2). While there is no straightforward trend and interpretation for the sign of $\Delta^b N(\Omega)$ and $\Delta^b \mu_z(\Omega)$, $\Delta^b Q_{zz}(\Omega)$ is positive for all the atoms displaying a significant variation ($|\Delta^b Q_{zz}(\Omega)|>0.01$ au). This means stacking interactions flatten $\rho(\mathbf{r})$ towards the molecular plane of monomers around all those atoms where $\Delta^b Q_{zz}(\Omega)>0$. $Sh(\Omega)$ depletions are also especially important in those atoms involved in intermolecular bond paths. The only significant enhacements observed for $Sh(\Omega)$ correspond to atoms placed far from the stacked region (H1''(Me)^m and H7(Me)^m). Table 6 shows that atoms experiencing significant enhancements of $Q_{zz}(\Omega)$ display important negative $\Delta^b Sh(\Omega)$ values, indicating $\Delta^b Q_{zz}(\Omega)$ acts for them as the main origin for the relative increase in the uniformity of $\rho(\mathbf{r})$ affecting monomers upon stacking interaction. We remark there is a big contrast between these values in stacking (Table 6) and IHB complexes (Table 4). Thus, in IHB-adducts: i) $\Delta^b \mu(\Omega)$ absolute values are much larger and their amount does not allow to infer proximity to any IHB; ii) In contrast, $\Delta^b Sh(\Omega)$ largest variations allow to identify the atoms involved in main IHBs; iii) $\Delta^b Q_{zz}(\Omega)$ values do not show the common depletion observed in atoms involved in stacked complexes.

This flattening can be also inferred from the variations in the scalar moments of $\rho(\mathbf{r})$, whose summations, $\Sigma\Delta^b r^1(\Omega)$ and $\Sigma\Delta^b r^2(\Omega)$, are negative for both monomers (Table 7), indicating $\rho(\mathbf{r})$ approaches, in average, the nucleus of basins and turns into a more

spherical distribution after complex formation. Variations experienced upon binding by atomic volumes $v_1(\Omega)$ and $v_2(\Omega)$ and by the electron population enclosed by them indicate this $\rho(\mathbf{r})$-flattening affects mainly to the diffuse electron density distributed far from the nuclei. Accordingly, $\Sigma\Delta^b v_1(\Omega)$ is negative and $\Sigma\Delta^b v_2(\Omega)$ is positive for both monomers, showing the volume occupied by the electron density between $2\cdot10^{-3}$ and $1\cdot10^{-3}$ au has decreased upon stacking. At the same time $\Sigma\Delta^b N_1(\Omega)$ is exceeded by $\Sigma\Delta^b N_2(\Omega)$, so the electron population enclosed in **M** and **C** monomers between $2\cdot10^{-3}$ and $1\cdot10^{-3}$ au isosurfaces, $\Sigma\Delta^b N_{12}(\Omega)$, has also decreased upon stacking. Furthermore, decrease of diffuse electron density is also pointed out by the depletion of $Sh(\Omega)$ (Table 7). Globally, the summations of property variations (Table 7) along monomers confirm there is global CT between monomers ($\Sigma\Delta^b N(\Omega)$=0.007 au) and indicate there is a slight global polarization which moves the centre of $\rho(\mathbf{r})$ away from the intermolecular region ($\Sigma\Delta^b \mu_z(\Omega)$=-0.112 and 0.092 au for atomic basins in **C** and in **M** monomers, respectively). As a result, $\rho(\mathbf{r})$ flattens with regard to an axis orthogonal to the molecular plane of each monomer ($\Sigma\Delta^b Q_{zz}(\Omega)$= 1.31 and 1.16 au for **M** and **C**, respectively).

Looking at Figure 4b, it is noticeable that the small variations observed for $\Delta^b N(\Omega)$ agree with the small magnitude achieved by $\Delta\rho(\mathbf{r})$. We have to choose very low isosurfaces (below 0.001 au in absolute value) to obtain meaningful regions for the latter. $\Delta\rho(\mathbf{r})$ plot shows enhancement and depletion regions around all the atoms involved in bond paths. In agreement with the description provided by $\Delta^b N(\Omega)$, $\Delta^b \mu_z(\Omega)$, and $\Delta^b Q_{zz}(\Omega)$ values, the alteration of $\rho(\mathbf{r})$ upon stacking interactions is more related to the distortion of electron distributions in atomic basins than to transfer of electron density from one basin to another. In the **M** monomer most of the enhanced $\rho(\mathbf{r})$ regions

are located around H1(Me) and O1''(sp^2) nuclei. The most depleted regions correspond to N7, C7 and H7 basins in **C**.

Despite the fact that $\Delta\rho(\mathbf{r})$ plot indicates nearly no depletions in the intermolecular area (H1(Me) and O1''(sp^2) being the exceptions), $\Sigma\Delta^{b}N_{12}(\Omega)$ values lead us to believe the intermolecular enhancements areas are collecting the most diffuse electron density of the intermolecular region. Overall, all areas where $\Delta\rho(\mathbf{r})$ is significant do not correspond to the region where monomers, delimited according to a certain $\rho(\mathbf{r})$ isosurface, e.g. 10^{-3} au, overlap.

On the basis of global CT among monomers, cooperative effects between face to face complexes, estimated considering complexes **8** and **9** (Figure 2), could be described as nearly negligible. Thus global CT in complexes displaying two face to face arrangement **8** and **9** (0.016 and 0.014 au, respectively) is very close to the summation of those found for the corresponding isolated face to face interactions shown in **6** and **7**. In both cases the electron density is removed from **M** monomers and transferred to **C** ones. Moreover, for these complexes, $\Delta^{b}N(\Omega)$ values, as well as those of other atomic properties, seem to be in line with those detailed for complex **6**.

The set of out of plane bond paths established in complexes **6-9** (Figure 2) confirm the trifling character of cooperative effects for stacking interactions. Thus, every **M**···**C** pair is connected by seven bond paths. As commented above, two different sets of bond paths are found depending on the arrangement adopted by the methyl groups of the central monomer with regard to its out of plane neighbor. Both sets are observed in complexes **8** and **9**. Inclusion of a second face to face interaction does not modify the BCP properties of intermolecular bond paths in a significant extent. For example, differences in $\rho(\mathbf{r}_c)$ values do not exceed $2\cdot10^{-4}$ au (Table 5).

Combination of hydrogen bonding and face to face interactions (10-11). Interplay between IHB and stacking interactions is present in the crystalline structure of caffeine methyl gallate adduct.[6] This situation has been modeled by means of complexes **10** and **11** (Figure 3). $\Delta^{b}N(\Omega)$ values computed for these compounds reveal cooperative effects are more significant when the central monomer is **M** than for **C**. Thus, in **10**, the electron density taken from the central **C** monomer (-0.060 au) is quite well matched by the balance between computed CT for complexes **4** (-0.073 au) and **8** (0.016 au). In contrast, the electron density gained by the central **M** monomer in complex **11** (0.040 au), differs more than 40% from that obtained from the balance of the corresponding CTs in complexes **5** (0.071 au) and **9** (-0.014 au).

QTAIM molecular graphs obtained for complexes **10** and **11** contain all the bond paths shown in IHB complexes **4**-**5** and face to face trimers **8**-**9**, but also, some new bond paths established between in-plane and out-of-plane neighbors (Figure 3). These molecular graphs provide an explanation for the cooperative effects exhibited by the CT of complex **11**. Thus, both the number and the $\rho(\mathbf{r}_c)$ values, of intermolecular bond paths among **C** in-plane and out-of-plane units in complex **11** exceed those displayed among the corresponding **M** units in complex **10** (Table 8) . In contrast, the properties of the bond critical points associated to **M**···**C** interactions do not display significant differences with those observed in smaller size complexes (**1**-**9**).

Conclusions

QTAIM electron density analysis and electron density deformation plots indicate significant differences between the electron density reorganization involved in IHB and π-π interactions. For H-bonding complexes we notice:

i) Every IHB complex contains one O-H···X (X=O, N) IHB and several C-H···O bond paths.

ii) In all cases IHB complexes display electron density transfer from **C** to **M** unit/s.

iii) The electron density transferred from **C** to **M** is provided by atoms of **C** not directly involved in IHB, while the population of those involved is enhanced upon IHB complexation.

iv) Deformation density plots indicate the largest reorganization of $\rho(\mathbf{r})$ takes place around the strongest IHB bond path.

In contrast, the following features are characteristic of π-π complexation:

i) The electron distribution of nearly all the basins of both monomers are more ordered (meaning closer to a uniform distribution) after the formation of the adduct, as indicated by negative $\Delta^{b}Sh(\Omega)$ values. The only exceptions are those atoms in the furthest positions with regard to the other monomer.

ii) Atomic electronic dipole moments vary significantly for many basins. These variations are due to the z-component (orthogonal to the plane of both monomers) of the dipole moment of the monomers ($\Sigma\Delta^{b}\mu_{z}(\Omega)$ is 0.092 au in **M** and -0.112 au in **C**).

iii) The zz element of the electronic quadrupoles of all the basins, but those furthest away from the other monomer (OCH_3 group of **M** and O6 in **C**), increase upon complexation. This indicates that the adduct formation has been accompanied by a certain flattening of the prolate spheroid representing the electron density analogue of π population. Therefore, the π population becomes more concentrated towards the corresponding π nodal plane in each monomer upon stacking complexation.

Finally, the only significant cooperative effects observed in complexes involving several strong IHBs and stacking interactions correspond to cases where intermolecular bondpaths between homomonomers are observed.

References

(1) E. A. Meyer, R. K. Castellano and F. Diederich, *Angew. Chem., Int. Ed.*, 2003, **42**, 1210.

(2) (a) K. Nakamura and K. N. Houk, *Org. Lett.*, 1999, **1**, 2049. (b) J. Ribas, E. Cubero, F. J. Luque and M. Orozco, *J. Org. Chem.*, 2002, **67**, 7057.

(3) (a) P. M. Felker, P. M. Maxton and M. W. Schaeffer, *Chem. Rev.*, 1994, **94**, 1787. (b) K. R. Leopold, G. T. Fraser, S. E. Novick and W. Klemperer, *Chem. Rev.*, 1994, **94**, 1807. (c) K. Mueller-Dethlefs, O. Dopfer and T. G. Wright, *Chem. Rev.*, 1994, **94**, 1845. (d) M. J. Elrod and R. J. Saykally, *Chem. Rev. (Washington, D. C.)*, 1994, **94**, 1975. (e) S. Sun and E. R. Bernstein, *J. Phys. Chem.*, 1996, **100**, 13348. (f) K. Mueller-Dethlefs and P. Hobza, *Chem. Rev.*, 2000, **100**, 143.

(4) Y. P. Yurenko, J. Novotny, V. Sklenar and R. Marek, *Phys. Chem. Chem. Phys.*, 2014, **16**, 2072.

(5) Y. Zhao, D. G. Truhlar, *J. Phys. Chem. A*, 2005, **109**, 4209.

(6) R. Martin, T. H. Lilley, N. A. Bailey, C. P. Falshaw, E. Haslam, D. Magnolato and M. J. Begley, *J. Chem. Soc., Chem. Commun.*, 1986, 105.

(7) D. T. Hurts, in An Introduction to the Chemistry and Biochemistry of Pyrimidines, Purines and Pteridines, Wiley, New York, 1980.

(8) E. Haslam, in Practical Polyphenolics: from Structure to Molecular Recognition and Physiological Action, Cambridge University Press, Cambridge, 1998.

(9) Y. Cai, Y, R. Martin, T. H. Lilley, E. Haslam, S. H. Gaffney, C. M. Spencer, D. Magnolato, *J. Chem. Soc. Perkin Trans*. *2*, 1990, 2197.

(10) R. F. W. Bader, *Chem. Rev.*, 1991, **91**, 893.

(11) R. F. W. Bader, in Atoms in Molecules, a Quantum Theory; Oxford University Press, New York, 1990.

(12) C. Matta, R. J. Boyd, in The Quantum Theory of Atoms in Molecules: from Solid State to DNA and Drug Design; WILEY-VCH, Weinham, 2007.

(13) K. B. Wiberg, R. F. W. Bader, C. D. H. Lau, *J. Am. Chem. Soc.*, 1987, **109**, 985.

(14) K. B Wiberg, R. F. W. Bader, C. D. H. Lau, *J. Am. Chem. Soc.*, 1987, **109**, 1001.

(15) M. Mandado, A. Vila, A. M. Grana, R. A. Mosquera and J. Cioslowski, *Chem. Phys. Lett.*, 2003, **371**, 739.

(16) F. Cortes-Guzman and R. F. W. Bader, *Chem. Phys. Lett.*, 2003, **379**, 183.

(17) R. F. W. Bader, P. L. A. Popelier, T. A. Keith, *Angew. Chem. Int. Ed. Engl.*, 1994, **33**, 620.

(18) D. Ferro-Costas, N. Otero, A. M. Graña, R. A. Mosquera, *J. Comput. Chem.*, 2012, **33**, 2533.

(19) F. Cortés-Guzmán, J. Hernández-Trujillo, G. Cuevas, *J. Phys. Chem. A*, 2003, **107**, 9253.

(20) M. T Caroll, C. Chang, R. F. W. Bader, *Mol. Phys.*, 1988, **63**, 387.

(21) M. T. Caroll, R. F. W. Bader, *Mol. Phys.*, 1988, **65**, 695.

(22) U. Koch, P. L. A. Popelier, *J. Phys. Chem.*, 1995, **99**, 9747.

(23) S. Grabowski, (ed.), in Hydrogen Bonding – New Insights, Springer-Verlag, 2006.

(24) A. Vila, R. A. Mosquera, *J. Phys. Chem. A*, 2006, **110**, 11752.

(25) R. F. W. Bader, *J. Phys. Chem. A*, 1998, **102**, 7314.

(26) M. J. González Moa, M. Mandado, R. A. Mosquera, *J. Phys. Chem. A*, 2007, **111**, 1998.

(27) Y. Zhao, D. G. Truhlar, *J. Phys. Chem. A*, 2004, **108**, 6908.

(28) M. J. Frisch, G. W. Trucks, H. B. Schlegel, G. E. Scuseria, M. A. Robb, J. R. Cheeseman, J. A. Montgomery, T. V. Jr., K. N. Kudin, J. C. Burant, J. M. Millam, S. S.

Iyengar, J. Tomasi, V. Barone, B. Mennucci, M. Cossi, G. Scalmani, N. Rega, G. A. Petersson, H. Nakatsuji, M. Hada, M. Ehara, K. Toyota, R. Fukuda, J. Hasegawa, M. Ishida, T. Nakajima, Y. Honda, O. Kitao, H. Nakai, M. Klene, X. Li, J. E. Knox, H. P. Hratchian, J. B. Cross, V. Bakken, C. Adamo, J. Jaramillo, R. Gomperts, R. E. Stratmann, O. Yazyev, A. J. Austin, R. Cammi, C. Pomelli, J. W. Ochterski, P. Y. Ayala, K. Morokuma, G. A. Voth, P. Salvador, J. J. Dannenberg, V. G. Zakrzewski, S. Dapprich, A. D. Daniels, M. C. Strain, O. Farkas, D. K. Malick, A. D. Rabuck, K. Raghavachari, J. B. Foresman, J. V. Ortiz, Q. Cui, A. G. Baboul, S. Clifford, J. Cioslowski, B. B. Stefanov, G. Liu, A. Liashenko, P. Piskorz, I. Komaromi, R. L. Martin, D. J. Fox, T. Keith, M. A. Al-Laham, C. Y. Peng, A. Nanayakkara, M. Challacombe, P. M. W. Gill, B. Johnson, W. Chen, M. W. Wong, C. Gonzalez and J. A. Pople, Gaussian 03, Revision C.02, Gaussian, Inc., Wallingford CT, 2004.

(29) R. F. W. Bader, in AIMPAC: A suite of programs for the theory of atoms in molecules, Mc Master University, Hamilton, Ontario, Canada, 1994.

(30) F. W. Biegler-König, J. Schönbohm, D. Bayles, *J. Comp. Chem.*, 2001, **22**, 545.

(31) D. Cremer, E. Kraka, *Croat. Chem. Acta*, 1984, **57**, 1259.

(32) M. Hô, V. H. Jr. Smith, D. F. Weaver, C. Gatti, R. P. Sagar, R. O. Esquivel, *J. Chem. Phys.*, 1998, **108**, 5469.

(33) M. Hô, B. J. Clark, V. H. Jr. Smith, D. F. Weaver, C. Gatti, R. P. Sagar, R. O. Esquivel, *J. Chem. Phys.*, 2000, **112**, 7572.

(34) C. F. Matta, N. Castillo, R. J. Boyd, *J. Phys. Chem. B*, 2006, **110**, 563.

(35) L. Estévez, N. Otero, R. A. Mosquera, *J. Phys. Chem. A*, 2009, **113**, 11051.

(36) A. Vila, R. A. Mosquera, *Chem. Phys*., 2003, **291**, 73.

(37) A. Robertazzi, J. A. Platts, *J. Phys. Chem. A*, 2006, **110**, 3992.

(38) M. P. Waller, A. Robertazzi, J. A. Platts, D. E. Hibbs, *J. Comput. Chem.*, 2006, **27**, 491.

1

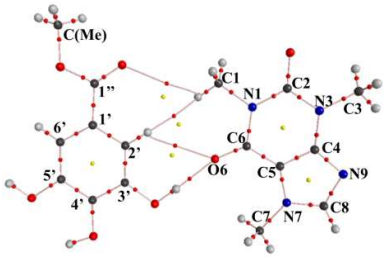

2

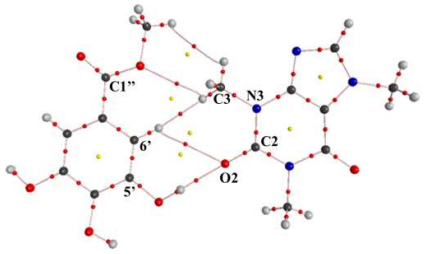

3

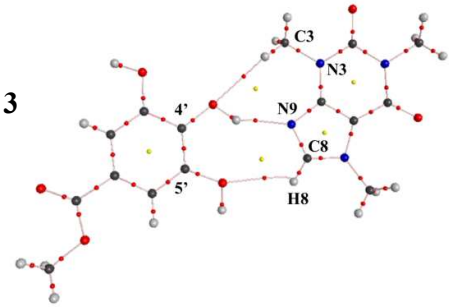

4

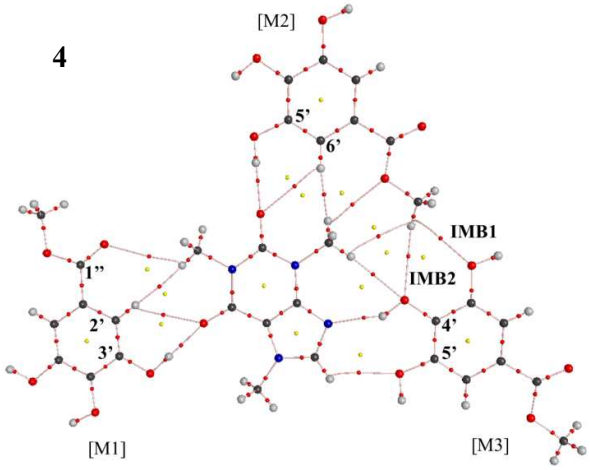

5

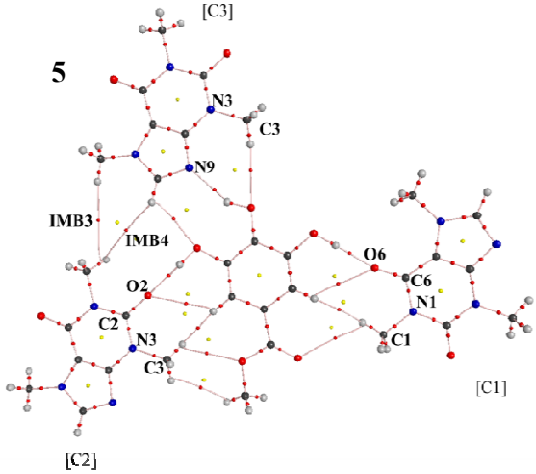

Figure 1. AIM2000 molecular graphs for non-stacked H-bonding systems studied in this work (**1**-**5**), showing intermolecular bond paths and critical points for $\rho(\mathbf{r})$. BCPs are red circles and ring critical points (RCP) yellow ones. Atomic numbering for monomers is shown in complex **1**. IMB1 to IMB4 denote BCPs associated to bond paths established between surrounding monomers in, **4** and **5**, with no equivalent BCP in complexes **1**-**3**. Their $\rho(\mathbf{r}_c)$ values are, respectively, 8.9, 5.6, 0.8 and 0.6 (in au multiplied by 10^3). Symbols in brackets in complexes **4**-**5** denote the binary **M**···**C** complex with an equivalent non-central monomer. Atom numbering for **C** and **M** is shown in complex **1**. The numbering for atoms involved in main IHBs is also shown in complexes **2**-**5**.

6

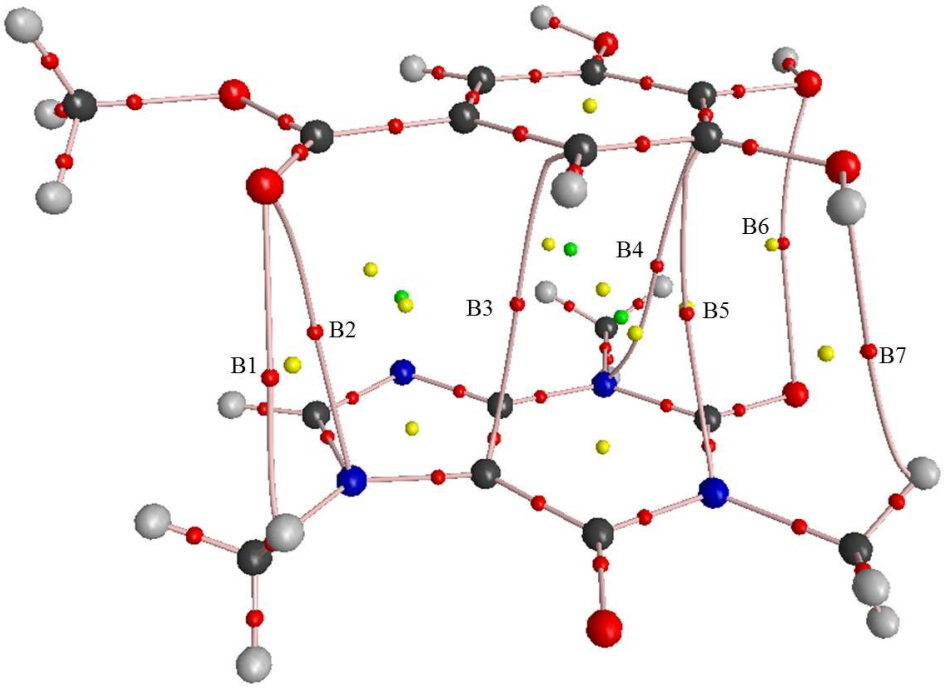

7

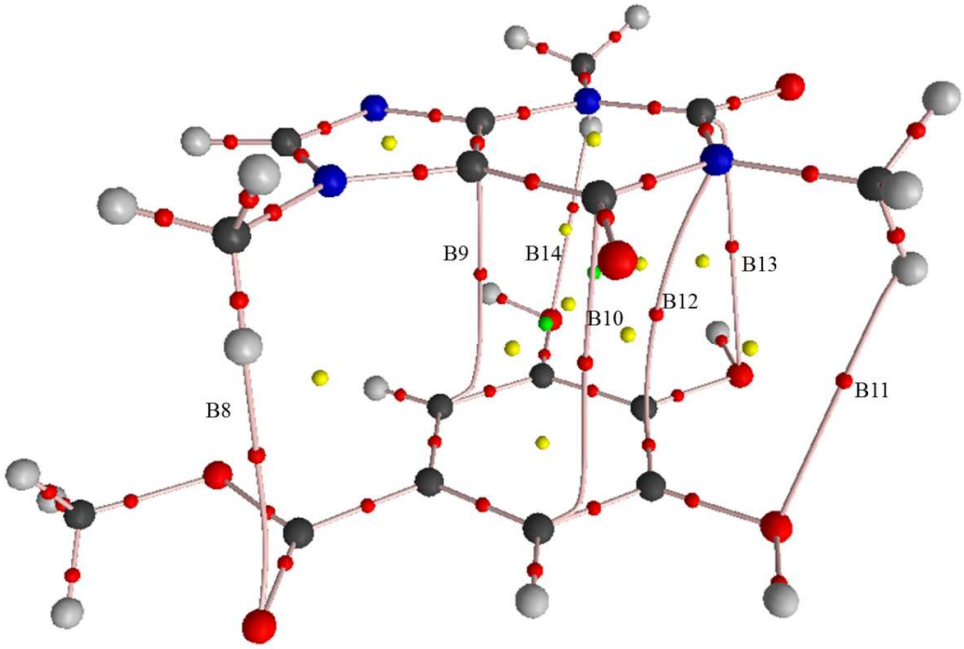

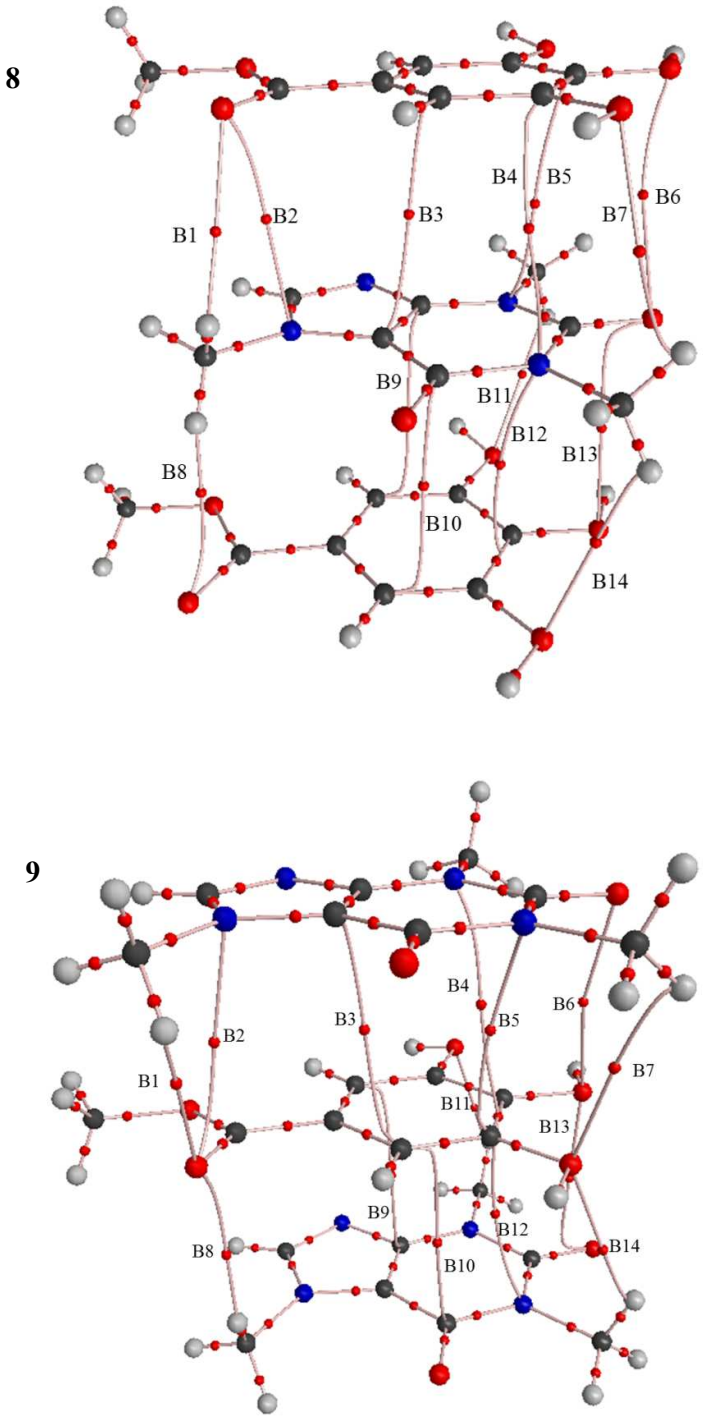

Figure 2. AIM2000 molecular graphs for stacked complexes studied in this work (**6-9**), showing intermolecular bond paths and critical points for $\rho(\mathbf{r})$. Circles in red are BCPs, RCPs in yellow and cage critical points (CCP) in green. For simplicity RCPs and CCPs are not shown in **8** and **9**.

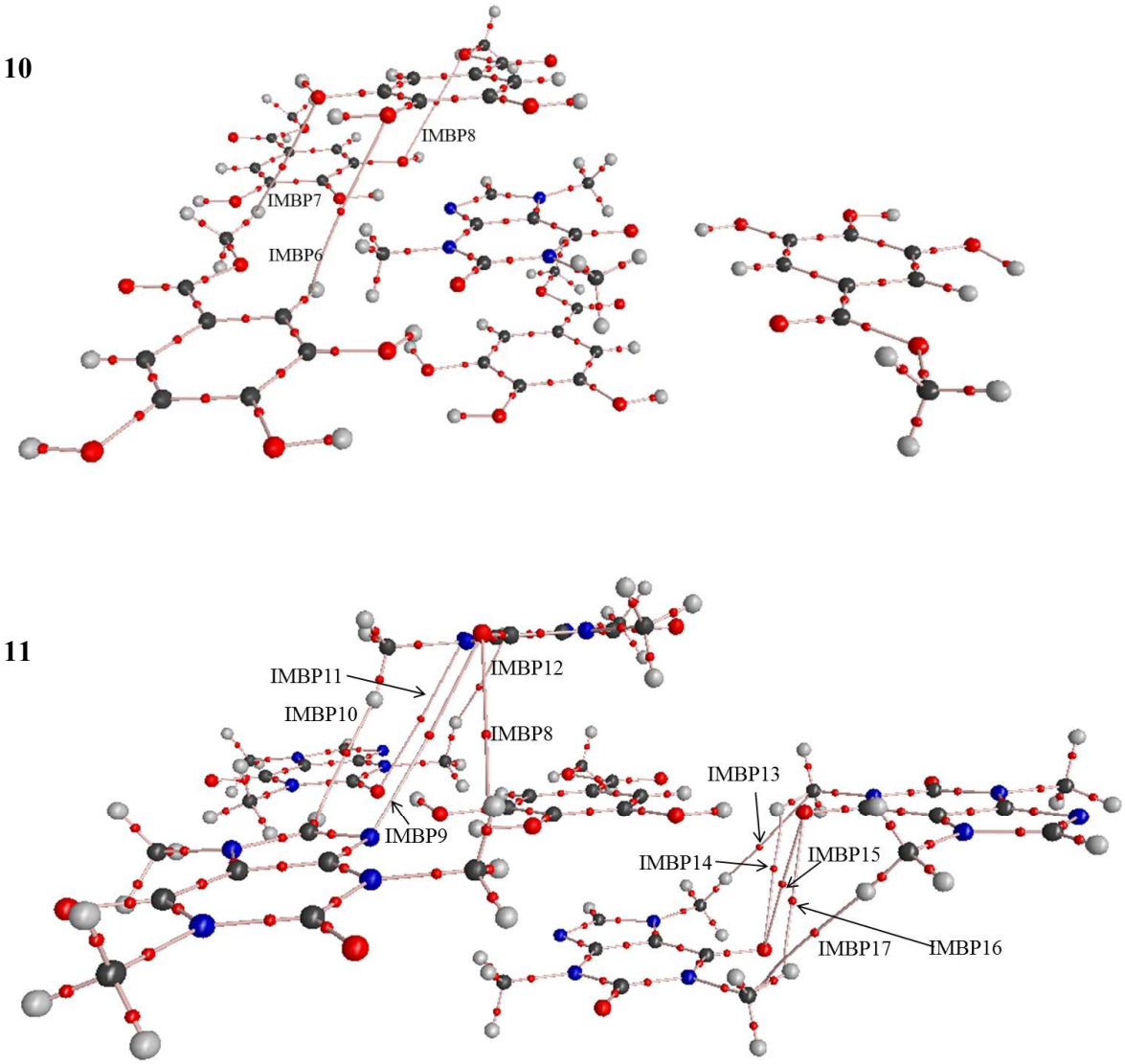

Figure 3. AIM2000 molecular graphs for complexes **10** and **11**, showing intermolecular bond paths not present in complexes **1-9** (Table 8). Circles in red are BCPs, RCPs and CCPs not shown.

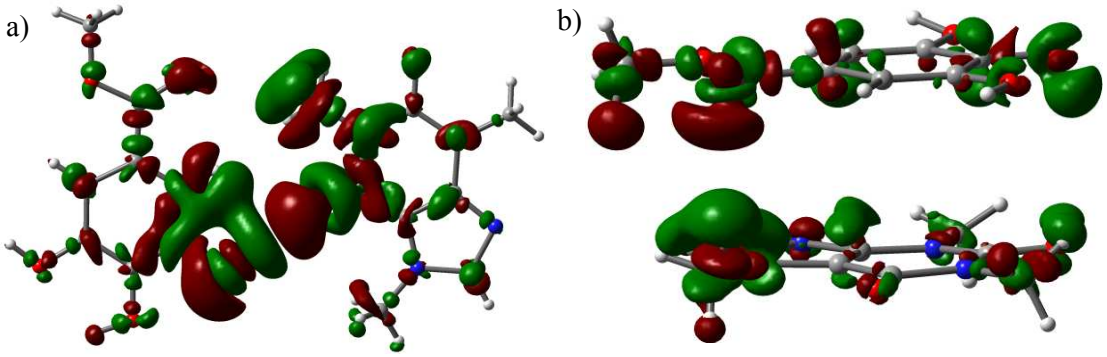

Figure 4. Deformation density plots for IHB complex **1** (a) and face to face **M**···**C** adduct **6** (b). Green and red denote, respectively, $4 \cdot 10^{-4}$ au and $-4 \cdot 10^{-4}$ au isosurfaces.

Table 1. Molecular energies (in au) and binding energies (in kJ mol^{-1}) computed at the MPW1B95/6-311++G(2d,2p) 6d level for all systems studied here.

	E	$\Delta^b E$
C	-680.16400	
M	-685.68429	
1	-1365.86245	-37.2
2	-1365.85961	-29.7
3	-1365.85652	-21.6
4	-2737.25318	-95.3
5	-2726.21076	-90.5
6	-1365.85432	-15.9
7	-1365.85689	-22.6
8	-2051.54726	-38.5
9	-2046.02615	-36.4
10	-4108.64268	-150.2
11	-4086.55268	-127.1

Table 2. Main properties of intermolecular BCPs found in complexes **1-3** (Figure 1) and variations experienced by $\rho(\mathbf{r}_c)$ in compounds 4 and 5 with regard to the dimer with the same bond path ($\Delta^4\rho(\mathbf{r}_c)$ and $\Delta^5\rho(\mathbf{r}_c)$). All values in au but internuclear distances, R, in Å. Main IHBs in boldface.

	BCP	$10^3\rho(\mathbf{r}_c)$	$10^3\nabla^2\rho(\mathbf{r}_c)$	$10^3H(\mathbf{r}_c)$	R	$10^3\Delta^4\rho(\mathbf{r}_c)$	$10^3\Delta^5\rho(\mathbf{r}_c)$
	O3'-H3'···O6	31.1	117.7	1.1	1.781	-0.07	0.00
1	C2'-H2'···O6	7.2	26.3	1.0	2.631	-0.02	0.02
	C1-H1···H2'	5.1	18.6	0.9	2.257	0.00	0.04
	C1-H1···O1''(sp^2)	3.6	13.7	0.7	2.969	0.00	0.00
	O5'-H5'···O2	26.5	106.6	2.0	1.837	-0.07	0.07
2	C1-H1···O1''(sp^3)	9.0	35.9	1.5	2.538	-0.03	-0.01
	C6-H6···O1(sp^3)	10.9	40.9	1.7	1.905	-0.01	0.04
	O1'(sp^3)C-H···H-C3	4.4	17.2	1.0	2.468	-0.18	0.00
	C6'-H6'···O2	6.4	22.5	0.9	2.723	0.00	0.00
	O4'-H4'···N9	25.6	77.7	0.7	1.988	-0.07	-0.11
3	C8-H8···O5'	7.6	30.9	1.3	2.547	-0.01	0.01
	C7-H7···O4'	7.5	29.9	1.2	2.474	0.05	0.02

Table 3. Atomic electron populations, $N(\Omega)$, (in au) in the isolated monomers (**C** and **M**) for the basins involved in the strongest IHB in **1-3.** Variations (in au multiplied by 10^3) due to binding in **1**-**3**, Δ^b, and cooperative effects, Δ^c, in complexes **4** and **5** are also shown.

	Ω	$N(\Omega)^a$	$\Delta^b N(\Omega)$	$\Delta^{c4} N(\Omega)$	$\Delta^{c5} N(\Omega)$
	C3'	5.437	-20	-18	-9
	O3'	9.130	43	60	64
1	H3'	0.415	-58	-63	-61
	O6	9.163	40	30	37
	C5'	5.501	-19	-19	-8
2	O5'	9.151	60	42	49
	H5'	0.399	-65	-56	-50
	O2	9.180	36	25	36
	C4'	5.429	-9	-7	5
3	O4'	9.118	44	51	51
	H4'	0.394	-37	-37	-36
	N9	8.014	24	17	14

[a]Values in isolated monomers
[c4]Cooperative effects in complex **4** (3 **M** + 1 **C**)
[c5]Cooperative effects in complex **5** (1 **M** + 3 **C**)

Table 4. Variations of selected atomic properties in the formation of **C**···**M** adduct **1** computed from MPW1B95/6-311++G(2d,2p) 6d electron densities. All values in au multiplied by 10^3, but $\Delta^b Q_{zz}(\Omega)$ in au multiplied by 10^2.

	Caffeine						Methyl gallate				
Ω	$\Delta^b N(\Omega)$	$\Delta^b Sh(\Omega)$	$\Delta^b Q_{zz}(\Omega)$	$\Delta^b r^I(\Omega)$	$\Delta^b \mu(\Omega)$	Ω	$\Delta^b N(\Omega)$	$\Delta^b Sh\Omega)$	$\Delta^b Q_{zz}(\Omega)$	$\Delta^b r^I(\Omega)$	$\Delta^b \mu(\Omega)$
C1	8	1	-6	5	-11	C1'	5	3	-4	11	9
C2	-4	-3	85	-7	-220	C1"	4	1	181	3	740
C3	3	-1	220	-2	-200	C(Me')	0	-1	297	-5	-317
C4	-4	-3	89	-11	-105	C2'	4	0	-335	1	-277
C5	-3	-1	-164	-5	-74	C3'	-19	-9	-123	-35	-96
C6	4	5	3	13	406	C4'	12	4	38	18	588
C7	5	2	-2	8	14	C5'	8	3	-18	12	-31
C8	-1	2	-221	-7	196	C6'	2	1	-42	5	-598
H1(Me)^t	-7	-40	9	-19	-10	H(Me')^g	1	3	-1	2	-16
H1(Me)^g	-9	-10	15	-13	9	H(Me')^t	1	2	-11	1	-19
H1(Me)^m	-16	-20	17	-23	-12	H(Me')^m	2	2	30	2	-64
H3(Me)^t	-3	-3	-30	-4	2	H2'	-17	-66	-70	-37	12
H3(Me)^g	-2	-2	-2	-3	6	H3'	-65	-394	9	-87	-14
H3(Me)^m	-3	-4	34	-4	9	H4'	3	8	-3	4	9
H7 (Me)^t	-6	-6	-46	-9	3	H5'	3	8	37	3	34
H7(Me)^g	-1	2	20	2	31	H6'	8	8	0	11	1
H7(Me)^m	-5	-7	40	-7	-24	O"(sp^2)	12	1	50	15	172
H8	-5	-7	-62	-8	-23	O"(sp^3)	-2	0	-5	-2	-26
N1	-1	-1	-44	-3	-67	O3'	60	18	-51	113	-181
N3	0	0	-40	0	-110	O4'	2	2	1	8	75
N7	-1	0	52	-2	49	O5'	3	1	0	7	-45
N9	-7	-2	44	-15	108						
O2	-9	-3	-8	-18	5						
O6	40	-10	-10	15	-4						

[a] Methyl hydrogens are labeled t, g, m indicating approximate values for the following dihedral angles: H1-C1-N1-C2 (158.9º, 41.1º and -77.1º, respectively), H3-C3-N3-C4 (142.7º, 16.7º and -98.3º, respectively), H7-C7-N7-C5 (162.7º, 47.6º and -72.1º, respectively), and H-C-O(sp2)-C1" (154.6º, 39.7º and -80.7º, respectively) dihedral angles.

Table 5. Main properties (in au) of the BCP found in stacked complexes **6** and **7** (Figure 2) and variations experienced by $\rho(\mathbf{r}_c)$ in compounds 8 and 9 with regard to them ($\Delta^{8}\rho(\mathbf{r}_c)$ and $\Delta^{9}\rho(\mathbf{r}_c)$). All values in au., but internuclear distances, R, in Å.

	BCP	Bond path	$10^3\rho(\mathbf{r}_c)$	$10^3\nabla^2\rho(\mathbf{r}_c)$	$10^3H(\mathbf{r}_c)$	R	$10^3\Delta^{8}\rho(\mathbf{r}_c)$	$10^3\Delta^{9}\rho(\mathbf{r}_c)$
6	B1	O1''(sp^2)···H7	4.8	19.5	0.9	2.849	-0.01	-0.03
6	B2	O1''(sp^2)···N7	4.7	17.4	0.8	3.352	-0.02	-0.03
6	B3	C2'···C5	5.3	14.9	0.8	3.501	-0.00	-0.02
6	B4	C4'···N3	4.1	13.6	0.7	3.587	-0.01	-0.02
6	B5	C3'···N1	3.8	13.4	0.7	3.571	-0.02	-0.00
6	B6	O4'···O2	2.5	10.8	0.6	3.575	-0.00	-0.02
6	B7	O3'···H1	3.2	13.0	0.7	3.062	0.01	-0.01
7	B8	O1''(sp^2)···N7	4.7	16.8	0.8	2.850	-0.05	-0.11
7	B9	C6'···C4	5.6	17.2	0.9	3.458	0.10	0.08
7	B10	C2'···C6	4.7	16.6	1.0	3.466	-0.02	-0.05
7	B11	O5'···H3	7.4	23.7	0.8	2.635	-0.17	-0.18
7	B12	C4'···N1	4.7	14.8	0.8	3.484	0.05	0.07
7	B13	O4'···C2	3.8	15.9	0.9	3.384	-0.12	-0.10
7	B14	O3'···H1	4.7	15.8	0.7	2.847	-0.13	-0.16

Table 6. Variations of selected atomic properties in the formation of caffeine···methyl gallate adduct **6** computed from MPW1B95/6-311++G(2d,2p) 6d electron densities. All values in au multiplied by 10^3, but $\Delta Q_{zz}(\Omega)$ in au multiplied by 10^2.

	Caffeine						Methyl gallate				
Ω^a	$\Delta^b N(\Omega)$	$\Delta^b Sh(\Omega)$	$\Delta^b Q_{zz}(\Omega)$	$\Delta^b \mu_z(\Omega)$	$\Delta^b \mu(\Omega)$	Ω^a	$\Delta^b N(\Omega)$	$\Delta^b Sh\Omega)$	$\Delta^b Q_{zz}(\Omega)$	$\Delta^b \mu_z(\Omega)$	$\Delta^b \mu(\Omega)$
C1	2	-1	1	4	3	C1'	-1	-6	14	19	19
C2	-2	-3	3	-4	-2	C1"	5	-1	4	-2	9
C3	-1	-4	6	0	-1	C(Me)	-3	-5	-1	5	-1
C4	-3	-6	9	-13	1	C2'	3	-8	20	13	4
C5	-4	-6	13	-16	-4	C3'	-1	-6	11	5	1
C6	3	0	2	1	3	C4'	-6	-10	17	10	-1
C7	2	0	3	9	11	C5'	2	-3	9	5	2
C8	-2	-6	9	-12	-6	C6'	-4	-7	20	16	6
H1(Me)^t	9	10	0	3	1	H1"(Me)^g	-5	-4	0	-1	0
H1(Me)^g	-8	-19	4	-4	-2	H1"(Me)^t	-2	-2	0	-2	0
H1(Me)^m	0	1	0	0	1	H1"(Me)^m	14	15	0	-5	5
H3(Me)^t	0	-10	5	-4	0	H2'	-2	-10	3	2	-1
H3(Me)^g	4	-1	3	-2	1	H3'	-1	-5	0	1	0
H3(Me)^m	2	4	0	-1	1	H4'	0	2	0	0	0
H7(Me)^t	1	-1	3	-6	3	H5'	-1	0	0	0	0
H7(Me)^g	-18	-36	6	-12	-4	H6'	-5	-8	2	4	-1
H7(Me)^m	9	9	0	-1	1	O1"(sp^2)	11	-3	14	-1	-1
H8	7	2	2	-3	0	O1"(sp^3)	-1	-1	-1	-6	7
N1	2	-2	7	-5	2	O3'	-1	-5	9	13	12
N3	1	-2	6	-6	3	O4'	-9	-5	5	19	15
N7	-3	-4	11	-14	-2	O5'	2	-1	4	-1	1
N9	8	-1	14	-13	5						
O2	-6	-5	11	-20	7						
O6	4	1	-1	6	-2						

[a] Methyl hydrogens are labeled t, g, m indicating the approximate values (see Table 4) for H1-C1-N1-C2, H3-C3-N3-C4, H7-C7-N7-C5, and H-C-O(sp2)-C1" dihedral angles. Notice, that the hydrogens in the intramonomer region of complex **6** are labeled with g and t superindices in **C**, but with m and g in **M**.

Table 7. Summations of variations of selected atomic properties in the formation of **C**···**M** complex **6** computed from MPW1B95/6-311++G(2d,2p) 6d electron densities. All values in au multiplied by 10^3, but $\Delta Q_{zz}(\Omega)$ (in au multiplied by 10^2) and $\Delta^b\nu(\Omega)$ (in au).

	$\Sigma\Delta^b N(\Omega)$	$\Sigma\Delta^b E(\Omega)$	$\Sigma\Delta^b Q_{zz}(\Omega)$	$\Sigma\Delta^b Sh(\Omega)$	$\Sigma\Delta^b r^1(\Omega)$	$\Sigma\Delta^b r^2(\Omega)$	$\Sigma\Delta^b \nu_1(\Omega)$	$\Sigma\Delta^b \nu_2(\Omega)$	$\Sigma\Delta^b N_{12}(\Omega)$
M	-7	507.5	131	-74	-141	-842	-16.0	15.1	-44
C	7	-516.2	116	-80	-67	-551	-9.1	18.1	-38

Table 8. Electron density at the BCP, $\rho(\mathbf{r}_c)$, (in au) of bond paths of complexes **10**-**11** with no equivalencies in **1**-**9.** All of them are found between in-plane and out-of-plane surrounding monomers (**M**···**M** in **10** and **C**···**C** in **11**).

	BCP	Bond Path	$10^3\rho(\mathbf{r}_c)$	$10^3\nabla^2\rho(\mathbf{r}_c)$	$10^3H(\mathbf{r}_c)$
10	B15	H6'···O4'	1.7	4.5	0.3
10	B16	H6'···O5'	1.1	7.3	0.5
10	B17	O5'…H(Me)	1.7	7.3	0.5
11	B18	N3-C-H···O2	0.7	2.9	0.2
11	B19	N9···O2	1.8	6.7	0.4
11	B20	C8-H···H-C3-N3	4.9	17.2	0.9
11	B21	O2···N9	1.9	6.7	0.4
11	B22	N3-C3-H···H-C8	4.9	17.1	0.9
11	B23	N1-C1···H-C7-N7	2.7	10.4	0.6
11	B24	N1-C1-H···O6-C6	3.1	12.0	0.6
11	B25	C6-O6···O2-C2	3.1	12.8	0.6
11	B26	C6-O6···H-C1-N1	3.2	12.0	0.6
11	B27	N7-C7-H···C1-N1	2.8	10.6	0.6